HiSST: 3rd International Conference on
High-Speed Vehicle Science Technology
14 -19 April 2024, Busan, Korea

Multi-objective Shape Optimization of Earth Re-Entry Capsule With Aero-Thermal Analysis

Minsul Lee[1], Kyu Hong Kim[2], Hyoungjin Kim[3]†

Abstract

In this study, multi-objective shape optimization of the re-entry capsule was conducted by using aero-thermal analysis engineering code. Capsule geometry was defined based on three-dimensional axisymmetric Viking geometry having five design parameters. Unstructured triangular surface mesh was automatically generated on surface geometries. The local surface inclination method and reference temperature method were used to estimate surface pressure and the skin friction coefficient. A streamline tracing method was implemented to calculate the local Reynolds number. Stagnation heat flux was estimated using the Brandis formula. Re-entry capsule geometry was optimized in the flow condition of Mach 24.7, angle of attack 0 deg, and altitude 50.63km using a multi-objective evolutionary algorithm, NSGA-Ⅲ. An optimum solution was selected among Pareto solutions considering the volumetric efficiency, drag area, and heat load as well as mass and ballistic coefficient.

Keywords: Hypersonic, Multi-objective optimization, Re-entry, Aero-thermal analysis

Nomenclature

CG – Center of Gravity
$\mathrm{L/D}$ – Lift-drag ratio
$\dot{q}$ – heat flux $[\mathrm{W/m^2}]$
R_c – Radius of corner [m]
R_n – Radius of nose [m]
S – Wetted surface area $[\mathrm{m^2}]$
η_v – Volume efficiency
θ – Angle w.r.t. symmetric axis [deg]
m – mass [kg]
A – reference area $[\mathrm{m^2}]$

1. Introduction

Attention to the study of space exploration has been increasing all over the world. To accomplish the space mission successfully, it is important to return the sample of the planet to Earth safely. And re-entry capsule can be used to return sample safely. When it comes to design of re-entry capsule, capsule needs to have a blunt nose to minimize heat load and a larger volume to load payload. Additionally, for a stable landing, it is needed to have good deceleration capabilities, and it is essential to maintain a low weight as a payload for a launch system. Generally, re-entry capsules can be categorized into two types based on the ballistic coefficient ($\beta = \frac{m}{C_D A}$).[1] The ballistic coefficient is calculated as the ratio of mass(m) to drag area($C_D A$). A ballistic capsule is characterized by a low ballistic coefficient value and refers to capsules re-entering in a zero-lift force. In contrast, lifting capsule typically re-enters with an angle of attack and are designed to have a non-zero lift-to-drag (L/D) ratio.

[1] *Dep't of Aerospace Engineering, Seoul National University, Seoul, Republic of Korea, minsul.lee@snu.ac.kr*
[2] *Dep't of Aerospace Engineering, Seoul National University, Seoul, Republic of Korea, aerocfd1@snu.ac.kr*
[3] *Dep't of Mechanical Engineering, Kyung Hee University, Yongin, Republic of Korea, hyoungjin.kim@khu.ac.kr*

† *Corresponding author*

In the re-entry phase, the capsule flies at hypersonic speed, therefore surface temperature of the vehicle will be getting higher due to the aero-heating phenomenon. Thus, in terms of shape optimization, not only aerodynamic analysis but also thermal analysis should be considered.

In this study, shape optimization for ballistic Earth re-entry capsule was performed with drag area, heat load, and volumetric efficiency as objective functions. A baseline configuration was selected as a Stardust-like capsule. The design variables consisted of five shape parameters, and the flow conditions were determined at a point where dynamic pressure is maximum based on the Stardust trajectory. The optimization utilized the DEAP library in Python and employed NSGA-Ⅲ. The Pareto front was analyzed to examine the shape characteristics corresponding to each objective function. Taking into account the capsule's mass and ballistic coefficient further with objective functions, optimal shape was proposed.

2. Methodology

2.1. Geometry

In this study, the geometric definition of a re-entry capsule was based on an axisymmetric three-dimensional Viking capsule.[2] The geometry was defined using five design parameters as depicted in Fig. 1. The radius of the capsule base was kept fixed as 0.2470 m as same as Stardust capsule [3].

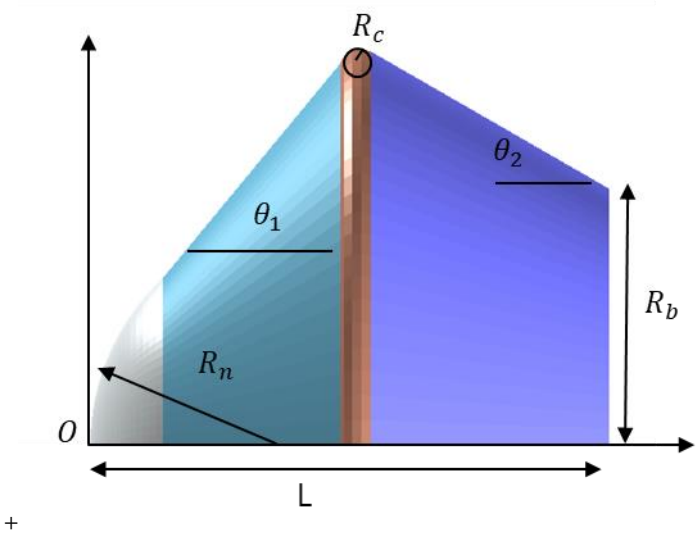

Fig 1. Re-entry capsule design parameters

Automatic surface meshing was implemented using a simple script that creates the structured plot3d format and converts it to unstructured triangular mesh. The domain was divided into five areas, including the base, and a grid of 100 points in the x-direction was established to create the surface mesh. In the shape module, the wetted area for each domain is calculated, along with the capsule's diameter and center of gravity. It was assumed that the center of gravity lies along the x-axis, and the volumetric center was calculated based on the assumption that larger volumes indicate more structures.

$$\bar{x} = \frac{\iiint x dV}{\iiint dV}$$

In this process, wetted surface area S and volume V was calculated using the created mesh. Then, the volumetric efficiency [4] was calculated as follows:

$$\eta_V = 6\sqrt{\pi}\frac{V}{S^{3/2}} .$$

2.2. Aerodynamic analysis

In the hypersonic regime, with the assumption of a thin shock layer, the oblique shock relation can be simplified. According to Newton's theory, particles impacting the surface lose their perpendicular momentum component while retaining their tangential component.[5] With this assumption, the pressure on the windward side can be calculated using the Modified Newtonian method [5]. And for the expansion side, the Sharma method which is a three-dimensional correction of the two-dimensional Prandtl-Meyer method was used.[6] Base pressure was assumed as vacuum condition.[7]

Windward:

$$C_P = k \sin^2 \delta$$

$$k = \frac{2}{\gamma M^2}\left(\frac{P}{P_\infty} - 1\right)$$

$$\frac{P}{P_\infty} = \left\{\frac{(\gamma+1)^2 M_\infty^2}{4\gamma M_\infty^2 - 2(\gamma-1)}\right\}^{\frac{\gamma}{\gamma-1}} \left\{\frac{1+\gamma+2\gamma M_\infty^2}{\gamma+1}\right\}$$

Leeward:

$$C_P = \frac{(C_P)_{cone}}{(C_P)_{wedge}} (C_P)_{Prandtl-Meyer}$$

Base:

$$C_P = \frac{1}{\gamma M_\infty^2}$$

Friction drag was calculated using Meador and Smart's reference temperature method[8]. The flow was assumed to be laminar, and streamline tracing techniques were used for local Reynolds number calculation.

Table 1. Design Flow conditions

Altitude	Mach	AoA
50.63 km	35	0 deg

2.3. Thermal analysis

The surface wall temperature was calculated under the assumption of radiative equilibrium condition. The wall temperature can be calculated iteratively using the energy balance equation[9].

$$\dot{q}_{conv} + \dot{q}_{rad} = \sigma \epsilon T_w^4$$

The calculation of heat flux was divided between stagnation and off-stagnation areas. The off-stagnation heat flux was estimated using Meador and Smart's reference temperature method and Reynolds analogy[8].

For the stagnation area, Brandis's formula [10] was used to consider both convective and radiation heat flux. The total heat flux for the stagnation is sum of convective and radiation heat flux.

$$\dot{q}_{conv} = 7.455 \times 10^{-9} \rho^{0.4705} V^{3.089} R^{-0.52} \left[\frac{\mathrm{W}}{\mathrm{cm}^2}\right] \quad (3km/s \leq V \leq 9.5\ km/s)$$

$$\dot{q}_{rad} = CR^a \rho^b f(V), \quad C = 3.416 \times 10^4 \left[\frac{W}{cm^2}\right]$$

$$a = \min(3.175 \times 10^6 V^{-1.80} \rho^{-0.1575}, amax), \qquad amax = \begin{cases} 0.61 & if\ 0 \leq r_n \leq 0.5 \\ 1.23 & if\ 0.5 < r_n \leq 2 \\ 0.49 & if\ 2 < r_n \leq 10 \end{cases}$$

$$b = 1.261$$

$$f(V) = -53.26 + \frac{6555}{(1 + (16000/V)^{8.25})}$$

2.4. Estimation of radius of curvature

The principal radii of curvature are required to calculated the stagnation heat flux. In this study, the surface fitting process was accomplished by approximating the surface with a quadratic function following Kindlmann's method[11]. The coefficients of the function were determined using a least squares method, which utilizes geometric data from neighboring nodes.

$$F(x, y, z) = a_1 x^2 + a_2 y^2 + a_3 z^2 + a_4 xy + a_5 yz + a_6 xz + a_7 x + a_8 y + a_9 z = 0$$

For axi-symmetric capsule design cases with zero angle of attack, the radius of curvature of the stagnation point is known a priori as the design parameter Rn. However, in order to take into account non-zero angle of attack design conditions or other general geometric parameterization methods in the future, the radius of curvature estimation routine was implemented in this code.

2.5. Mass estimation

The total mass of a re-entry capsule was estimated as a sum of structural, payload, forebody, backshell, and marginal mass[12]. The weight of the thermal protection system(TPS) on the forebody was calculated using material density, forebody wetted area, and TPS thickness. The TPS thickness was calculated using the formula which relates the velocity and heat load[13]. PICA was selected as the TPS material for the forebody. The payload of the vehicle was fixed as 22.5 kg. The marginal mass was set as 20% of the total mass. The total mass is calculated as follows:

$$m_{total} = m_{structure} + m_{payload} + m_{forebody} + m_{backshell} + m_{margin}$$

$$\delta_{TPS} = 1.8696 \times \left(\frac{Heat\ load}{V_\infty}\right) \text{[cm]}$$

$$m_{str} = (0.0232 \times q_\infty)^{0.1708} m_0$$

$$m_{backshell} = 0.14 m_0$$

$$m_{forebody} = \delta_{TPS} \rho_{PICA} S_{forebody}$$

2.6. Optimization

The problem definition and constraints are as follows:

$$\text{Minimize:} \quad \begin{pmatrix} Heat\ load \\ 1/\eta_V \\ 1/(C_D A) \end{pmatrix}$$

$$\text{Subject to:} \quad \begin{cases} C_{M_\alpha} < 0 \\ R_c \leq 0.05\ m \\ L \leq 1.0\ m \\ 10° \leq \theta_1, \theta_2 \leq 70° \\ Diameter \leq 2.0\ m \end{cases}$$

The objectives are to minimize heat load and maximize drag area ($C_D A$) and volumetric efficiency (η_V). The process for evaluation of objective functions and constraints is depicted in Figure 2. The multi-objective evolutionary algorithm, NSGA-Ⅲ, implemented in the open-source python library DEAP [14] was adopted to explore the design space. The optimization was conducted for 80 generations with a population size of 300.

Geometric parameters for the baseline configuration are presented in Table 2. The calculated objective functions and constraints of baseline geometry are presented in Table 3.

Table 2. Baseline geometry

$\mathbf{R_b}$	$\mathbf{R_n}$	$\mathbf{R_c}$	**L**	$\boldsymbol{\theta_1}$	$\boldsymbol{\theta_2}$
0.2740 m	0.22 m	0.02 m	0.499 m	50.5 °	30 °

Table 3. Objective functions and constraints evaluated for the baseline configuration

Parameter	**Value**
$C_D A$	0.5219 m^2
Heat load	1.66 MJ/s
η	0.8726
β	107.76 kg/m^2
Mass	56.24 kg
C_{M_α}	-0.1705
$\dot{q}_{stag}$	8.18 MW/m^2

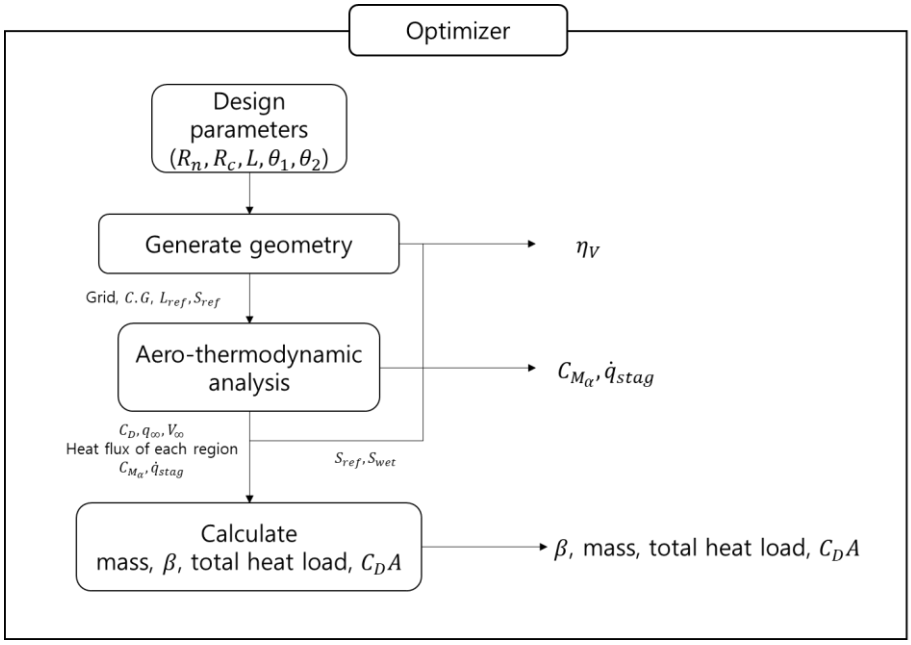

Fig 2. The procedure for evaluation of objective functions and constraints

3. Results

Figure 3 shows optimization results by NSGA-III, highlighting the pareto optimal solutions with a color bar. The optimization prioritized high volumetric efficiency, drag area and low heat load. Representative optimum solutions selected from the Pareto solutions are depicted in Fig.4, where shapes closer to a sphere (opt1, opt2) have much higher volumetric efficiency. A smaller forebody surface area correlates with minimum heat load (opt2, opt3, opt4, opt5), and a larger diameter indicates an increased drag area (opt6). Among the optimal solutions, those with reduced heat load and increased η_V and $C_D A$ compared to the baseline are marked in red in Figure 5.

It is observed that an increase in the forebody surface area of the re-entry capsule leads to a higher TPS weight, and consequently, a greater mass. Since a larger capsule frontal area ($C_D A$) tends to increase the forebody surface area, it can be inferred that this also results in an increased mass. Plotting the Pareto optimal solutions against mass and β shows the formation of a Pareto front. An optimum solution was selected minimizing the capsule mass while maximizing deceleration performance, considering a fixed payload weight. This approach ensures the most efficient design configuration, balancing minimum structural mass and maximum deceleration performance.

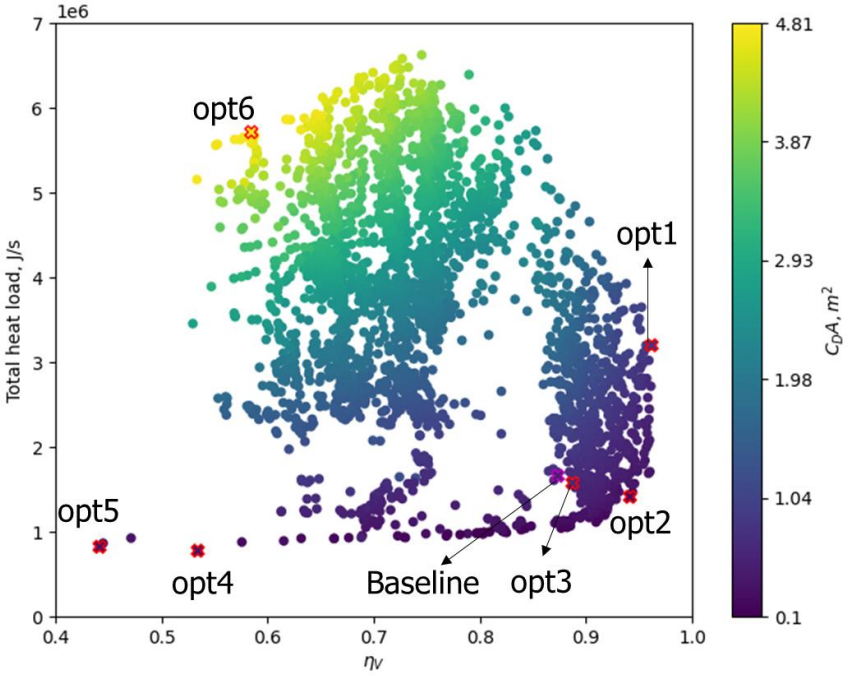

Fig 3. All pareto optimal solutions

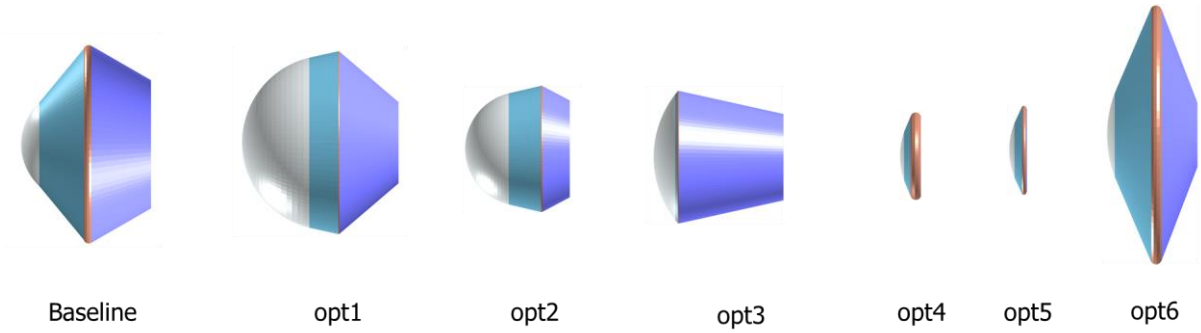

Fig 4. Geometries of representative optimum solutions

The geometric details of the optimum solution are presented in Table 4. In comparison to the baseline, it features a larger nose radius and frontal area. The objective function and constraints of the optimum solution are outlined in Table 5, revealing a reduction in stagnation point heat transfer, alongside enhanced deceleration capabilities. This improvement is attributed to the decreased surface area of the forebody, which consequently reduces the heat load.

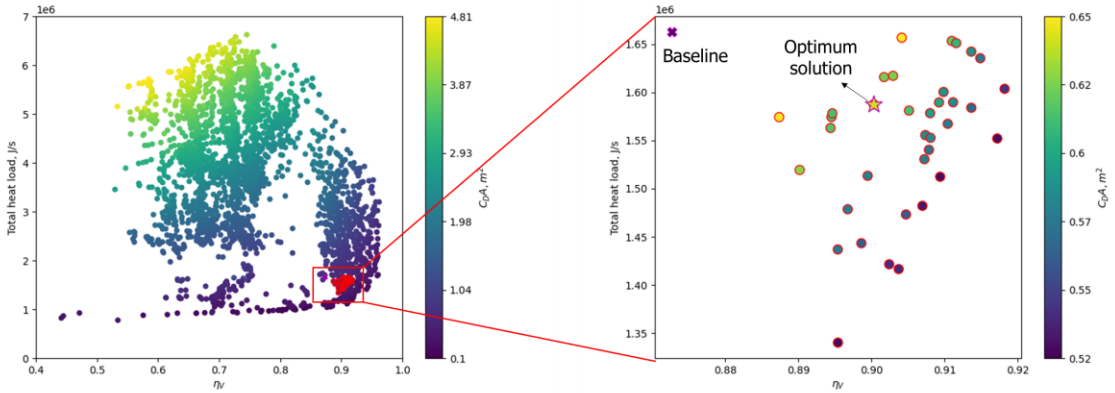

Fig 5. Pareto optimal solutions and a selected optimum solution

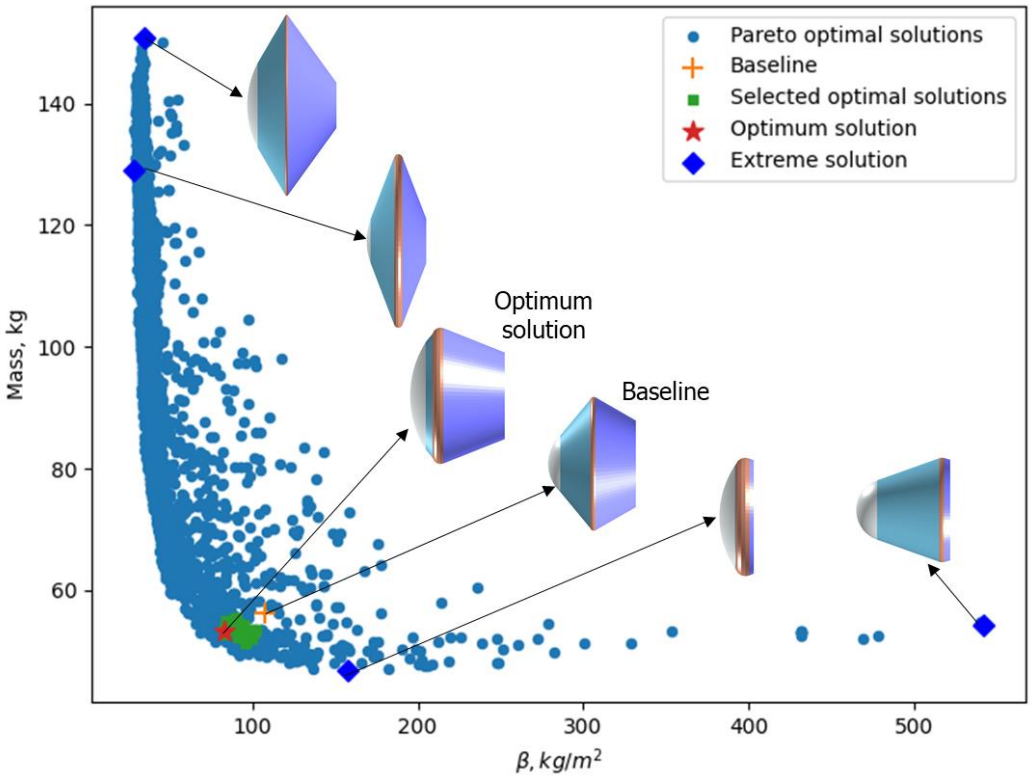

Fig 6. Mass vs β plot for Pareto optimal solutions

Table 4. Optimum solution

R_b	R_n	R_c	L	θ_1	θ_2
0.2740 m	0.5891m	0.0426m	0.6279m	48.16deg	15.72deg

Table 5. Optimum solution objective and constraint information

Parameter	Value
$C_D A$	0.6413 m^2 (+22.90%)
Heat load	1.59 MJ/s (-4.53%)
η	0.9003 (+3.17 %)
β	83.18 kg/m^2 (-22.82 %)
Mass	53.34 kg (-5.14 %)
C_{M_α}	-0.1278 (-25.01 %)
$\dot{q}_{stag}$	4.90 MW/m^2 (-40.05 %)

4. Conclusion

In this study, multi-disciplinary shape design optimization of re-entry capsules was conducted using a multi-objective evolutionary algorithm considering aero-thermal performance and volumetric efficiency. Aero-thermal analysis was conducted using an engineering code which uses the modified Newtonian method, reference temperature method, and Brandis's formula to calculate inviscid pressure, skin friction, and stagnation heat flux, respectively. Design objective were to minimize heat load and to maximize volumetric efficiency and drag area. A final optimum solution was selected among Pareto solutions considering mass and ballistic coefficient.

Acknowledgement

This work was supported by Korea Research Institute for defense Technology planning and advancement(KRIT) grant funded by the Korea government(DAPA(Defense Acquisition Program Administration)) (KRIT-CT-22-030, Reusable Unmanned Space Vehicle Research Center, 2024)

References

1. Hirschel, Ernst Heinrich; Weiland, Claus. Selected aerothermodynamic design problems of hypersonic flight vehicles. Springer Science & Business Media, (2009)
2. Cavallero, Claudio, et al. Multi-disciplinary shape optimization of an entry capsule integrated with custom neural network approximation and multi-delity approach. In: Eurogen 2011 Conference. (2011)
3. Boyd, Iain D.; Trumble, Kerry A.; Wright, Michael J. Modeling of stardust entry at high altitude, part 1: Flowfield analysis. Journal of Spacecraft and Rockets, 47.5: 708-717 (2010)
4. Thesinger, John E.; Braun, Robert D. Multi-objective hypersonic entry aeroshell shape optimization. Journal of Spacecraft and Rockets, 46.5: 957-966. (2009)
5. Anderson JD Jr, Hypersonic and high-temperature gas dynamics. American Institute of Aeronautics and Astronautics, Reston, Virginia (2006)
6. Sharma RK, Theerthamalai P, Panneerselvam S, Aerodynamic characteristics of forebody-c ylinder combinations of circular/non-circular cross section at angles of attack, Twelfth Austr alasian Fluid Mechanics Conference, University of Sydney, Australia, 695-698. (1995)
7. Sreekanth, A. K., Aerodynamic predictive methods and their validation in hypersonic flows. Defence Research & Development Organisation, Ministry of Defence
8. Meador, W. E., & Smart, M. K. Reference enthalpy method developed from solutions of the

boundary-layer equations. AIAA journal, 43(1), 135-139 (2005)

9. Kinney, D., Garcia, J., & Huynh, L. . Predicted convective and radiative aerothermodynamic environments for various reentry vehicles using CBAERO. In 44th AIAA Aerospace Sciences Meeting and Exhibit, p. 659 (2006)

10. Brandis, A. M., & Johnston, C. O., Characterization of stagnation-point heat flux for earth e ntry. In 45th AIAA Plasmadynamics and Lasers Conference, p. 2374, (2014)

11. Kindlmann, G., Whitaker, R., Tasdizen, T., & Moller, T., Curvature-based transfer functions for direct volume rendering: Methods and applications. In IEEE Visualization, 2003. pp. 51 3-520. IEEE. (2003)

12. Steinfeldt, B., Theisinger, J., Korzun, A., Clark, I., Grant, M., & Braun, R., High mass mars e ntry, descent, and landing architecture assessment. In AIAA Space 2009 Conference & Exp osition p. 6684. (2009)

13. Sepka, S., & Samareh, J. A., Thermal protection system mass estimating relationships for bl unt-body, earth entry spacecraft. In 45th AIAA Thermophysics Conference p. 2507, (2015)

14. Fortin, F. A., De Rainville, F. M., Gardner, M. A. G., Parizeau, M., & Gagné, C.: DEAP: Evolut ionary algorithms made easy. The Journal of Machine Learning Research, 13(1), 2171-2175. (2012)